Shape stability of deflated vesicles in general linear flows

Charlie Lin and Vivek Narsimhan*
Davidson School of Chemical Engineering, Purdue University, West Lafayette, Indiana 47907, USA

(Received 3 June 2019; published 26 December 2019)

The dynamics of vesicles in simple shear or extensional flows has been extensively studied, but the conditions where vesicles experience more complex flow types, such as those seen in microfluidic devices or industrial processing conditions, warrant greater investigation. In this study, we use the boundary element method to investigate the shape stability of deflated vesicles in a general linear flow, i.e., linear combinations of extensional and rotational flows. We model the vesicles as a droplet with an incompressible interface with a bending resistance. We simulate a range of flow types from purely shear to extensional at viscosity ratios ranging from 0.01 to 5.0 and reduced volumes from 0.60 to 0.70. The vesicle's viscosity ratio appears to play a minimal role in describing its shape and stability for many mixed flows, even in cases when significant flows are present in the vesicle interior. We find in these cases that the critical capillary number for shape instabilities collapses onto similar values if the capillary number is scaled by an effective extensional rate. These results contrast with droplet studies where both viscosity ratio and flow type have significant effects on breakup. Our simulations suggest that if the flow type is not close to pure shear flow, one can accurately quantify the shape and stability of vesicles using the results from an equiviscous vesicle in pure extension. When the flow type is nearly shear flow, we start to see deviations in the observations discussed above. In this situation, the vesicle's stationary shape develops asymmetric cusps, which introduces a stabilizing effect and makes the critical capillary number depend on the viscosity ratio.

DOI: 10.1103/PhysRevFluids.4.123606

I. INTRODUCTION

Vesicles are a paradigmatic model system for studying the dynamics of cellular systems. Part of the popularity of vesicles originates from their ease of manufacture through electroformation and their large size that can be easily tracked by optical microscopy [1,2]. The giant unilamellar vesicle (GUV) system is also similar in both size and composition to common anuclear cells. Giant unilamellar vesicles have been used to describe the motion of red blood cells [3,4], such as their tank-treading–tumbling and tumbling–vacillating-breathing behavior in shear flow [3,5]. From a more functional viewpoint, vesicles are vital components of countless biological processes including cellular digestion [6], cell signaling [7], or exocytosis [8]. Vesicles have also been directly applied to engineering applications such as biocompatible drug delivery [9,10] or microreactors for miniaturization studies [11,12]. Further motivation for vesicle research originates from the inability of droplet studies alone to describe all of the possible mechanics of vesicles or cells. Some of the differences include the possibility of nonspherical vesicle shapes at global equilibrium [13] and soft long-wavelength membrane fluctuations [2]. These numerous applications have prompted the biophysics community to be highly interested in studies examining the dynamics of vesicles.

*vnarsim@purdue.edu

Of interest is vesicle dynamics in external flows like those observed in microfluidic devices or biological systems. Previous research on vesicles in purely extensional flows includes the work by Kantsler *et al.,* who experimentally observed that highly deflated, high-aspect-ratio vesicles extend out into dumbbell-like shapes at extension rates above a critical value [14]. For intermediate-aspect-ratio vesicles, Spjut and Muller observed vesicles transitioning into an asymmetrical dumbbell shape at extension rates above a critical value [15,16]. Following these results, Shaqfeh and co-workers have done several computational and theoretical studies on the stability and transitional shapes observed for vesicles in extensional flow [17–20]. Some of the main conclusions from these studies include the negligible dependence of the critical extension rate on the viscosity ratio between the vesicle and the solution, and the importance of the steady-state shape on shape transitions under tension.

Few studies have examined deflated vesicles in general linear flows, i.e., linear combinations of rotational and extensional flows, even though the flow fields a vesicle will experience in complex geometries will not be perfectly shear or extensional. In such flows, determining the stability characteristics of vesicles is essential for manipulating vesicle dynamics.

In this paper, we use numerical simulations to probe the stability of deflated vesicles in a general linear flow field. There have been other experimental and theoretical studies examining vesicles in such flows, but they have focused on the motion of nearly spherical vesicles, characterizing the phase boundaries between tank-treading, tumbling, and the transitional regimes [3,21,22]. We note that studies on droplets in mixed flows have shown that the slender-drop and small deformation theories are close approximations of experimental results for critical extension rate, deformation, and orientation [23,24]; however, the stability of vesicles in such flows is qualitatively different from those observed for droplets. For example, droplets are known to break up readily in a wide range of flow types, but this does not appear to be the case for vesicles, which appear to be quite stable in nearly shear flows. Furthermore, internal viscosity appears to play a significant role in droplet breakup, but the simulations in this paper do not show such an effect for vesicles, even when significant internal flows are present. We will describe our simulation method, present our stability results, and explain our findings in the sections that follow.

II. MODEL AND METHODS

A. Governing equations

We model our system as a droplet surrounded by a two-dimensional incompressible fluid with a bending resistance. At the length scale of a GUV ($a \sim 10\ \mu$m) with deformation rates at $\dot{\epsilon} \sim 1\ \text{s}^{-1}$, the inner and outer fluids of the system are effectively very viscous with negligible inertial effects. This allows us to model the velocity field inside and outside the vesicle using the Stokes equations

$$\nabla \cdot \boldsymbol{u} = 0, \quad \nabla p = \mu \nabla^2 \boldsymbol{u}, \tag{1}$$

where $\boldsymbol{u}$ is the fluid velocity, p is the pressure, and μ is the fluid viscosity (μ_{in} for the inner fluid and μ_{out} for the outer fluid). The system is subject to continuity of velocity across the interface and a force balance across the phospholipid bilayer. The short timescales and low deformation rates used in previous studies make membrane dilatation negligible [25,26]. Vesicles are also known to have negligible shear rigidity as they do not have a cytoskeletal network or an actin cortex. We therefore choose to use the Helfrich model [27], a commonly used model that takes these factors into account,

$$\mathbb{H} = \oint \frac{\kappa}{2}(2H)^2 dA + \oint \sigma\, dA, \tag{2}$$

where $\mathbb{H}$ represents the elastic energy of the vesicle membrane, κ is the membrane bending modulus, H is the mean curvature, and σ is the surface tension. The surface tension is a spatially varying Lagrange multiplier that ensures local area conservation. Previous literature has shown that local area conservation leads to good global area incompressibility [28,29]. The surface tension enforces $\nabla_s \cdot \boldsymbol{u} = 0$ on the interface, where $\nabla_s = (\boldsymbol{I} - \boldsymbol{nn}) \cdot \nabla$. We note that the original

Helfrich model includes spontaneous curvature, a parameter to describe a membrane's curvature preference when the sides of the bilayer are chemically different. While vesicles *in vivo* may have multiple lipid components or chemical differences between the inner and outer fluids [30–32], experimental studies have focused on single-component vesicles with only a viscosity difference between the fluids, prompting a negligible spontaneous curvature. We have additionally neglected any contributions from thermal fluctuations, membrane viscosity, and bilayer friction [33,34].

At mechanical equilibrium, the force balance at the membrane surface becomes

$$[[\boldsymbol{f}]] = [[\boldsymbol{T}\cdot\boldsymbol{n}]] = \boldsymbol{f_t} + \boldsymbol{f_b} = (2H\sigma\boldsymbol{n} - \nabla_s\sigma) + \left[\kappa\left(4KH - 4H^3 - 2\nabla_s^2 H\right)\boldsymbol{n}\right], \tag{3}$$

where $[[\boldsymbol{f}]]$ is the jump in viscous traction across the interface which can be decomposed to the bending ($\boldsymbol{f_b}$) and tension ($\boldsymbol{f_t}$) contributions, $\boldsymbol{n}$ is the outward-pointing unit normal vector, and K is the Gaussian curvature of the interface. The mean curvature H is defined to be 1 for the unit sphere.

The vesicle is placed in an external linear flow field described by $\boldsymbol{u}^\infty = \nabla\boldsymbol{u}^\infty\cdot\boldsymbol{x}$. We define it as

$$\nabla\boldsymbol{u}^\infty = \frac{\dot\epsilon}{2}\begin{bmatrix}\alpha+1 & 1-\alpha & 0\\ \alpha-1 & -1-\alpha & 0\\ 0 & 0 & 0\end{bmatrix}, \tag{4}$$

where $\dot\epsilon$ is the deformation rate and α is a flow parameter that controls the flow type the vesicle experiences. The value $\alpha = 1$ corresponds to planar extensional flow, $\alpha = 0$ is shear flow, and $\alpha = -1$ is pure rotation. We additionally define an exit streamline as the eigenvector corresponding to the principal eigenvalue

$$\boldsymbol{b} = \left(\frac{-1-\sqrt{\alpha}}{-1+\sqrt{\alpha}}, -1\right), \quad \alpha \neq 1. \tag{5}$$

The membrane area A is kept constant by the incompressibility constraint, while the low permeability of the membrane allows us to assume that the volume V of the vesicle is constant during the timescale of experiments (minutes). Therefore, we nondimensionalize distances by the equivalent radius $a = \sqrt{A/4\pi}$, timescales by $\dot\epsilon^{-1}$, velocities by $\dot\epsilon a$, stresses by $\mu_{\text{out}}\dot\epsilon$, and surface tensions by $\mu_{\text{out}}\dot\epsilon a$. We obtain four dimensionless groups of interest from the nondimensionalization:

$$\text{Ca} \equiv \frac{\mu_{\text{out}}\dot\epsilon a^3}{\kappa}, \quad \lambda \equiv \frac{\mu_{\text{in}}}{\mu_{\text{out}}}, \quad \nu \equiv \frac{3V}{4\pi a^3}, \quad \alpha. \tag{6}$$

The capillary number Ca compares the bending timescale to flow timescale. Therefore, a high Ca would mean the vesicle shape is dominated by the external flow. The viscosity ratio λ is the ratio of inner and outer fluid viscosities. As cellular systems such as red blood cells commonly have a more viscous inner fluid, the parameter can be tuned to more closely model the system of choice. The reduced volume ν is a measure of the asphericity of the vesicle, or a measure of its osmotic deflation. For example, a reduced volume of 1 would be a perfect sphere, while a value of 0.2 would be highly deflated. One can experimentally alter the reduced volume of a vesicle by introducing an osmotic shock such as adding sucrose to the outer fluid. The flow parameter α was described earlier; it describes what type of mixed flow the vesicle will experience (pure rotation to pure extension). Applying this nondimensionalization, the force balance becomes

$$[[\boldsymbol{T}\cdot\boldsymbol{n}]] = \boldsymbol{f_t} + \text{Ca}^{-1}\boldsymbol{f_b}. \tag{7}$$

B. Boundary integral formulation

The Stokes flow assumption allows us to use the boundary integral, i.e., the Green's function, formulation to simulate the vesicle. We recast the Stokes equations into a boundary integral form

$$\frac{1+\lambda}{2}u_j(\boldsymbol{x}_0) = u_j^\infty(\boldsymbol{x}_0) - \frac{1}{8\pi}\int_S G_{ij}(\boldsymbol{x},\boldsymbol{x}_0)[[f_i]](\boldsymbol{x})dA(\boldsymbol{x}) + \frac{1-\lambda}{8\pi}\int_S T_{ijk}(\boldsymbol{x},\boldsymbol{x}_0)u_i(\boldsymbol{x})n_k(\boldsymbol{x})dA(\boldsymbol{x}), \tag{8}$$

where u_i^∞ is the external velocity field and $[[f_i]]$ is the jump in viscous traction across the interface, given by Eq. (7). The kernels $G_{ij}(\boldsymbol{x}, \boldsymbol{x}_0)$ and $T_{ijk}(\boldsymbol{x}, \boldsymbol{x}_0)$ are the Stokeslet (point force) and stresslet (point dipole) solutions to Stokes flow,

$$G_{ij}(\boldsymbol{x}, \boldsymbol{x}_0) = \frac{\delta_{ij}}{r} + \frac{\tilde{x}_i \tilde{x}_j}{r^3}, \tag{9}$$

$$T_{ijk}(\boldsymbol{x}, \boldsymbol{x}_0) = -6\frac{\tilde{x}_i \tilde{x}_j \tilde{x}_k}{r^5}, \tag{10}$$

where $\tilde{\boldsymbol{x}} = \boldsymbol{x} - \boldsymbol{x}_0$ and $r = |\tilde{\boldsymbol{x}}|$. Repeated indices are assumed to be summed in the above equations. These equations are also subject to the membrane incompressibility constraint

$$\nabla_s \cdot \boldsymbol{u} = 0. \tag{11}$$

Our simulations use code extended from Spann *et al.* [20]. The simulation procedure begins by discretizing the vesicle surface into an unstructured mesh of at least 5120 triangular elements. We solve for the velocity, pressure, and surface tension at each mesh point by using the predictor-corrector scheme from [35]. For computing the bending forces, we first approximate the curvature with Loop subdivision [20] and then apply the virtual work principle on the Helfrich energy functional [20]. After solving for the velocity at each mesh point, we translate the vertices by their normal velocity. The tangential velocity component is replaced by a mesh relaxation scheme similar to the one mentioned in Ref. [36]. Finally, we enforce the constant volume constraint by performing an affine transformation on the vesicle shape. This process is repeated until the desired amount of time has been simulated.

C. Vesicle shape stability

In this study, we examine the stability of a vesicle under a steady linear flow field. When a vesicle is deflated (reduced volume $0.58 < \nu < 0.75$), a vesicle under pure extension will transition to an asymmetric dumbbell above a critical capillary number (Fig. 1). The shape instabilities we examine in mixed flows will look similar to this process, although there will now be internal flows inside the vesicle due to the imposed vorticity. The asymmetric dumbbell deformation is assumed to grow indefinitely, suggesting breakup, but could also lead to additional stationary shapes. The origin of the asymmetric dumbbell instability is outlined in Ref. [18] but briefly, it arises due to the Laplace pressure induced in the pinched side of the vesicle, which drives flow toward the expanded side. Since the surface tension of the membrane is a function of the flow, this effect only occurs above a critical flow strength. To avoid highly deformed meshes and large capillary numbers, we decided to limit our simulations to the range of $\nu = 0.60$–0.70. We note that the history of the flow field, such as sudden increase in flow strength, could also affect vesicle stability, but the topic is outside the scope of the present paper.

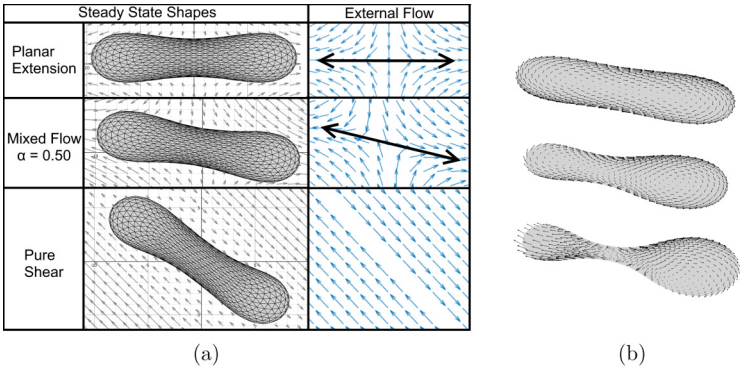

FIG. 1. (a) Steady-state vesicle shapes and the corresponding external velocities. The arrows correspond to the exit streamline. (b) Simulated asymmetrical instability and surface velocities.

The simulation procedure begins by first obtaining a vesicle at steady state, which is accomplished by simulating a prolate spheroidal mesh in external flow until the normal velocities at the vertices approach zero. This method differs from previous spectral simulations, which discarded the asymmetric contributions of the shape to obtain the equilibrium shape [17]. We then apply a small sinusoidal perturbation to the steady-state mesh and determine the conditions under which this perturbation will grow. Experimentally, this perturbation would occur spontaneously due to additional factors such as thermal fluctuations or minor flow perturbations. This perturbation is necessary for the simulation because, while our simulation does not automatically enforce symmetry, the minor asymmetries present in the finite mesh representation of the vesicle will not spontaneously start the instability for capillary numbers close to the critical value. The perturbation is defined as

$$r(z) = r_0(z) + \beta \sin(2\pi z/z_{\max}), \tag{12}$$

where r is the distance from the interface to the major axis of the vesicle shape and β is a small number, usually of order 0.01 times the original radius r_0. Visually, this perturbation makes one side of the vesicle slightly larger than the other (Fig. 1). Above a critical capillary number the perturbation will grow, while below the critical capillary number the perturbation will return to its steady configuration.

We note that the growth rate of the instability becomes increasingly small as the capillary number is near its critical value. This effect is significant because one typically has to simulate for long periods of time to visualize the instability at this transition. We decided to use a more robust method for determining the stability of a simulation by tracking the growth of the asymmetric perturbation. Previous simulations that tested vesicle stability in uniaxial extension were able to extract the Legendre polynomial representation of the vesicle shape and check the growth rate of the odd modes [17,20]. Our simulations of vesicles in mixed flows will not be radially symmetric, but we can do the same analysis for a $z = 0$ slice of the vesicle shape, i.e., the plane where flow occurs.

Our procedure consists of first projecting all the vertices onto the $z = 0$ plane and then using a concave hull algorithm [37] to select the vertices enclosing the projection. We record the distances from the vertices to the vesicle's major axis, rescale the points so that the end points of the major axis are at ± 1, and fit the shape to Legendre polynomials up to order 32 using the least-squares method. If the resultant coefficients for odd order polynomials consistently increase with time, we determine that the sinusoidal perturbation grows, eventually leading to the asymmetric instability. The even polynomial coefficients are constant until the shape becomes significantly deformed. This method allows us to determine the stability with fewer timesteps. An example of the odd Legendre coefficients is shown in Fig. 2.

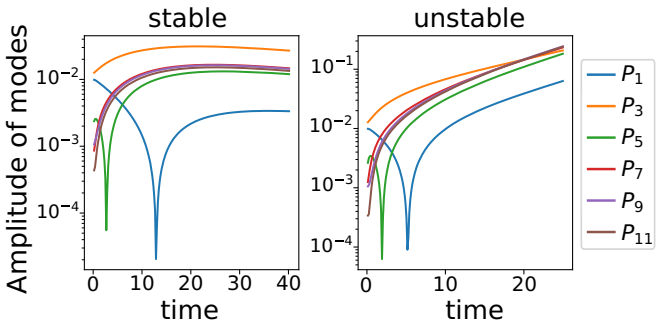

FIG. 2. Odd Legendre polynomials for a stable and an unstable simulation. The stable (unstable) simulation decreases (increases) exponentially after some transient initial effects. Mixed and extensional flows show qualitatively similar results for this analysis. The dips in the coefficients are some transient behavior and were also seen by Spann *et al.* [20].

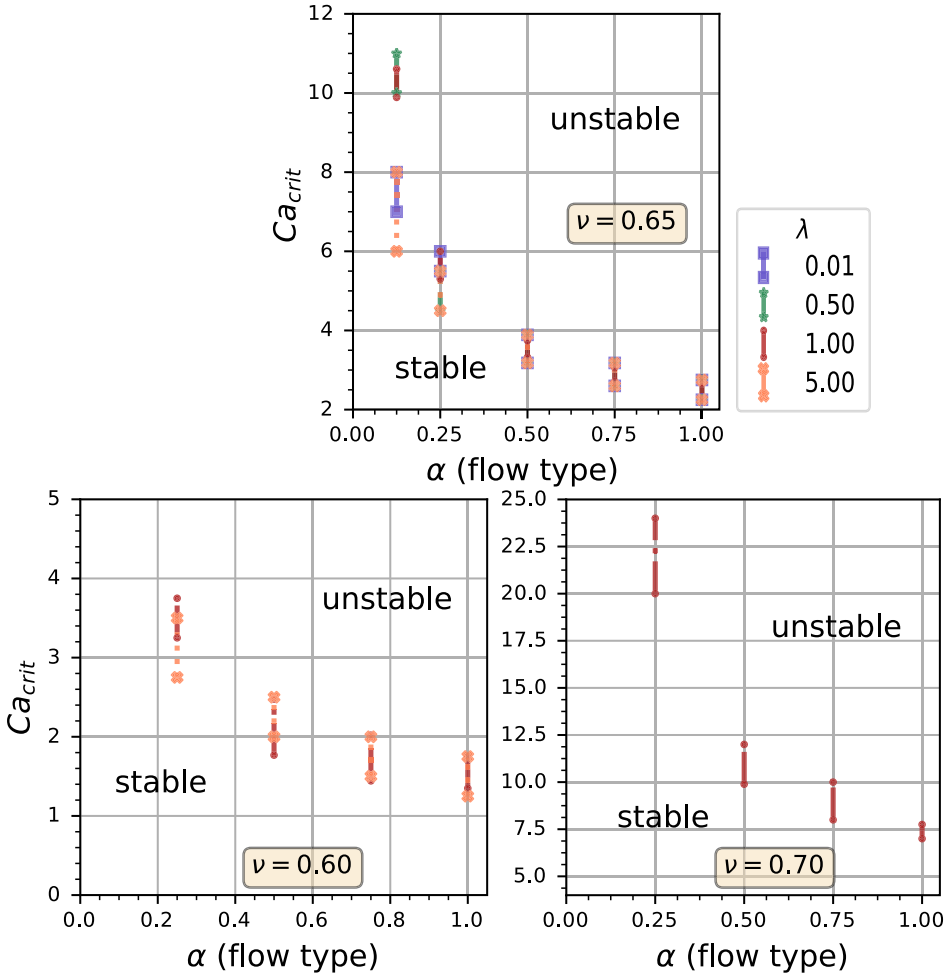

FIG. 3. Predicted stability boundaries for several reduced volumes ν and viscosity ratios λ. Several of the boundaries overlap exactly. All viscosity ratios were simulated for a reduced volume of 0.65. Simulations of viscosity ratios of 1.0 and 5.0 are shown for a reduced volume of 0.60. The boundaries for the reduced volume 0.70 runs are larger due to higher Ca requiring longer simulation times.

III. RESULTS AND DISCUSSION

The shape stability of a vesicle in pure planar extensional flow ($\alpha = 1$) has been studied extensively by Kantsler *et al.* and Dahl *et al.* in experiments [14,16], as well as in computational works by Shaqfeh and co-workers [17,20]. We benchmarked our simulations with the latter two studies and have been able to replicate their stability phase diagrams. This study focuses on mixed flows with an extensionally dominated component ($0 < \alpha < 1$). Figure 3 shows the stability boundary for vesicles in such flows over several reduced volumes ν and viscosity ratios λ. The critical capillary number diverges with a power-law behavior (exponent roughly 0.6) as the flow type approaches pure shear, i.e., $\alpha \to 0$, leading to no asymmetrical dumbbell deformations for purely shear flows. We note that this behavior is quite different from those observed for droplets, which can readily break up in shear flow if its interior viscosity is not too large [23,38].

Another interesting finding from the graphs is the dependence of vesicle stability on its viscosity ratio λ. In previous studies under pure extension ($\alpha = 1$), Narsimhan *et al.* showed that viscosity

ratio plays an inconsequential role in vesicle shape stability, since the vesicle experiences negligible flow in its interior due to membrane incompressibility [18]. The latter statement is not true in mixed flows, since external vorticity leads to substantial circulation in the vesicle interior. However, the viscosity ratio has a negligible effect on vesicle stability over a wide range of mixed flows, with a deviation occurring close to the pure shear flow ($\alpha = 0$) limit. This observation is in contrast to what is observed for droplet suspensions where the internal fluid plays a significant role in breakup [24].

To explain the power-law dependence of vesicle stability on flow type, we begin with some observations. First, all unstable vesicles we simulated have been in the tank-treading regime. We tracked the orientation angle of the vesicles over time and found that all of them stay constant after reaching their steady-state orientation. One can simulate the tumbling and vacillating-breathing regimes by further increasing the viscosity ratio or decreasing α. The majority of the relevant stability boundary will be in the tank-treading regime however, as the rotation timescale for the vacillating-breathing–tumbling regimes will likely be significantly smaller than the inverse growth rate of the asymmetrical instability, leading to no perceived shape instability. Note that the results for $\lambda = 5.0$ suggest that the critical viscosity ratio for the tank-treading–tumbling transition is affected by the flow type. We have not examined this effect in this study.

Second, the orientation of the tank-treading vesicles determines the effective extension it experiences. We define the effective extension as

$$\dot{\epsilon}_{\text{eff}} = \boldsymbol{c} \cdot \nabla \boldsymbol{u}^{\infty} \cdot \boldsymbol{c} = \dot{\epsilon}\left(\frac{1+\alpha}{2}\right)\cos(2\theta), \quad 0 < \theta < \pi, \tag{13}$$

where θ is the orientation angle of the vesicle and $\boldsymbol{c}$ is the major axis of the ellipsoidal vesicle. The vesicle will experience maximum extension when aligned with the x axis ($\theta = 0^{\circ}$) and a minimum extension when aligned at $\theta = -45^{\circ}$. We can redefine our capillary number based on this effective extension rate

$$\text{Ca}_{\text{eff}} = \left(\frac{1+\alpha}{2}\right)\cos(2\theta)\text{Ca}, \tag{14}$$

but this representation requires the orientation angle, which is not known *a priori*. Instead, we observe from Fig. 4 that the vesicles align closely with the exit streamline of the mixed flow, i.e., the eigenvector of Eq. (4) with a positive eigenvalue, for flow types not close to shear flow. The inclination angle differs by at most 4° from the exit streamline for $\alpha \geqslant 0.250$, suggesting that $\boldsymbol{c} \approx \boldsymbol{b}$. This observation and the approximate power-law exponent of roughly 0.60 motivate us to reexamine our data by scaling the capillary number by the effective extension rate along the exit streamline, which is $\sqrt{\alpha}\dot{\epsilon}$. The resultant dimensionless parameter corresponds to the effective capillary number along the exit streamline:

$$\text{Ca}_s = \sqrt{\alpha}\text{Ca}. \tag{15}$$

Once applying this scaling in Fig. 5, we observe that most of the stability boundary becomes invariant with flow type. These results suggest that the stability of vesicles of any viscosity ratio can be explained by the purely extensional case and a scaled deformation rate if the flow type is $\alpha \geqslant 0.500$. The stability boundary only begins to diverge from a purely effective extensional effect at close to pure shear flow ($\alpha = 0$).

This simple geometric argument for deflated vesicles is remarkable, since it is well known that droplets do not always align well with the flow principal axis. Significant differences in droplet orientation angle have been observed in several experiments, e.g., [24,39], and help explain why the stability boundary's dependence on flow type and viscosity ratio has a much more complicated relationship for droplets than the geometric arguments listed above. We note that for vesicles, the orientation angle can deviate greatly from the exit streamline, but this effect only appears important when its shape is quasispherical ($\nu > 0.80$) or when the flow type is nearly shear flow. A good reference for studies in the quasispherical regimes is in Refs. [40–42] and a good reference for

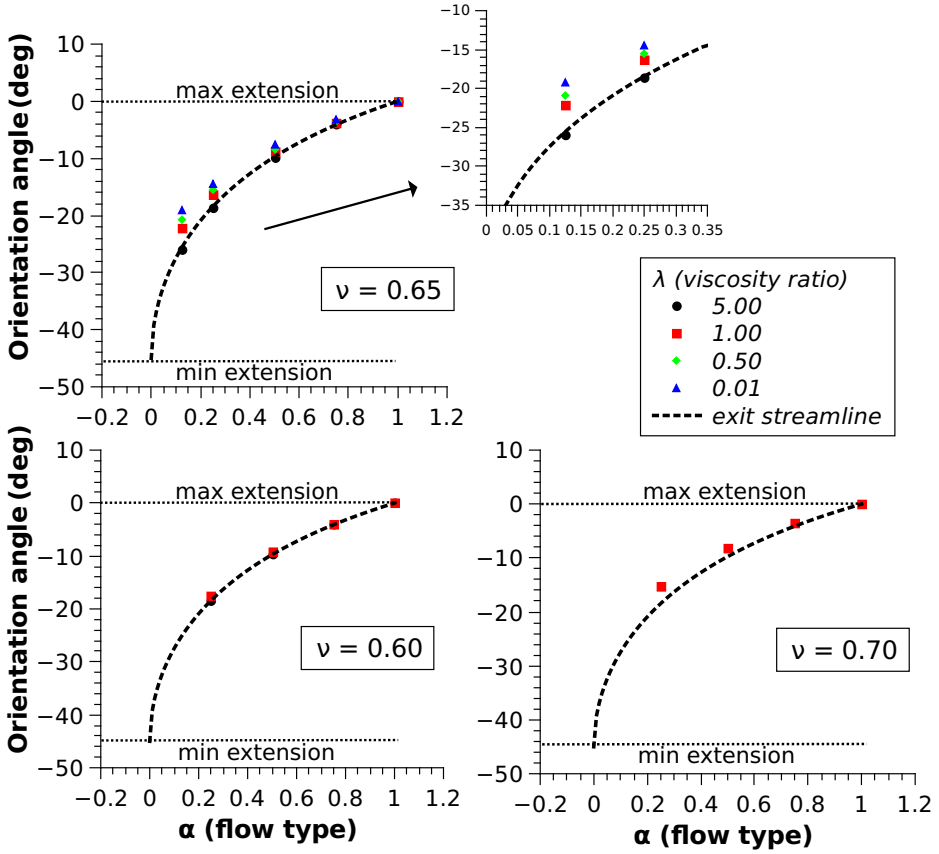

FIG. 4. Orientation angle of vesicle simulations compared to the exit streamline for vesicles near the stability boundary. The inset focuses on the low-α regime for $\nu = 0.65$.

low reduced volume vesicles or cells in shear flow is [43]. In our study, the asymmetric dumbbell instabilities occur at reduced volumes $0.58 < \nu < 0.75$ and the flow types significantly away from pure shear, which allows one to make the simple geometry arguments listed above.

In the last part of this section, we will make a few more statements that illuminate the physics of the shape instabilities in mixed flows. In previous studies, researchers found that the asymmetric dumbbell shapes arise from a competition between bending forces that try to stabilize the vesicle and membrane tension that tries to destabilize the vesicle. The first effect is primarily due to geometry, i.e., curvature of the membrane, while the latter effect is coupled through the flow. For more information on vesicle stability in mixed flows, we decided to measure the steady-state vesicle geometry and tensions near the stability boundary.

To begin our analysis, we focus on the moderate- to high-α regime ($\alpha \geqslant 0.500$). Let us examine two vesicles with $\mathrm{Ca}_s = 3.00$, $\nu = 0.65$, and $\lambda = 1$; one is in pure extension $\alpha = 1$ and the other is in a mixed flow at $\alpha = 0.5$. Although both vesicles will experience the same effective extension, the vorticity will be noticeably different, leading to different flow patterns in and around the vesicle. How do these flow patterns affect the vesicle shape? We plot the shapes of the two vesicles overlaying each other in Fig. 6(a). Overall, the shapes are almost identical, suggesting that the internal circulation induced by vorticity does not appreciably alter vesicle shape at moderate flow parameter α. Vesicles of the same shape have the exact same bending forces; therefore the stabilizing force for the instability will be the same.

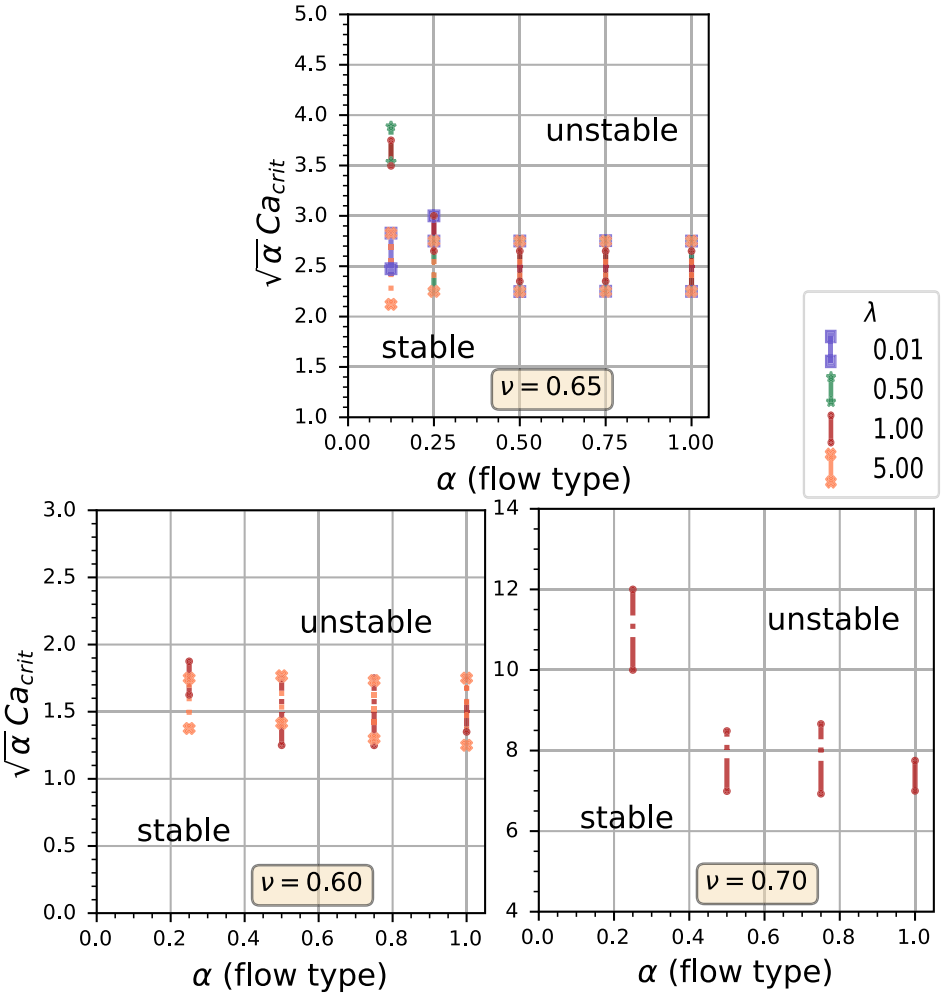

FIG. 5. Rescaled stability boundaries by $\sqrt{\alpha}$, corresponding to the effective extension along the exit streamline.

We plotted the maximum tension profile along the major axis of the vesicle of the same case in Fig. 7. From that figure we see that the tension profile is also invariant for $\alpha \geqslant 0.500$ at the same scaled capillary number. Overall, the tension profile is similar for most flow types except near shear flow ($\alpha \leqslant 0.25$). From Fig. 7 we also observe that the tension profile is independent of the viscosity ratio for $\alpha \geqslant 0.500$. These results suggest that the internal flows in the vesicle do not play a significant role in modifying the tension on the membrane, most likely because such flows are primarily rotational and hence do not stretch the material elements in the membrane appreciably. With both the membrane bending and tension contributions invariant at the same scaled capillary number for moderate-α values, we conclude that the vorticity has no significant effect in this regime. Additionally, the stability is independent of the flows internal to the vesicle, and hence does not depend on λ.

When vesicles approach pure shear flow ($\alpha = 0$), we notice that flow type and viscosity ratio start having significant consequences on its stability. To understand the role of these parameters in this regime, we examine the vesicle's shape and orientation. In Fig. 4, we observe that that vesicles with higher viscosity ratios align more closely with the exit streamline than those with lower viscosity

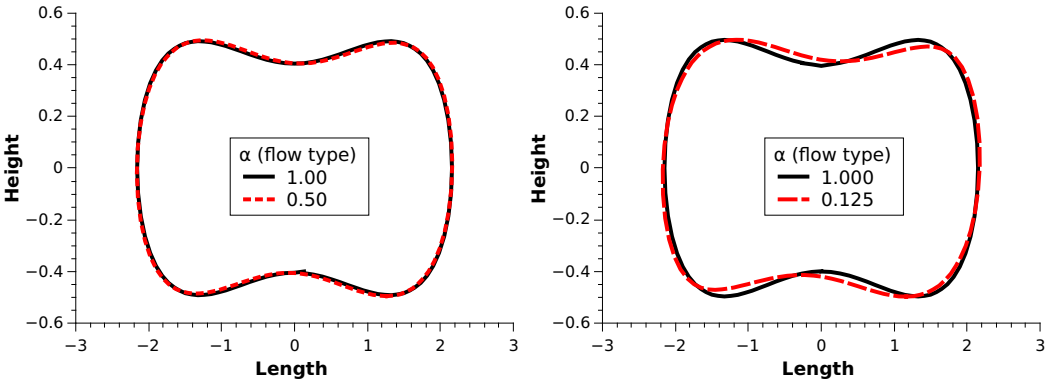

FIG. 6. Comparison of the stationary vesicle shape for vesicles in a purely extensional flow to those seen in mixed flows. Both plots have the parameters $\lambda = 1.00$ and $\mathrm{Ca}_s = 3.00$. (a) The $\alpha = 0.500$ flow results in a stationary shape that closely follows the extensional case. (b) The $\alpha = 0.125$ stationary shape deviates significantly from the extensional case. The y-axis scaling for (b) has been increased to make the shape deviation more noticeable.

ratios. This orientation effect leads to the more viscous vesicles experiencing a lower effective extension (Fig. 4), which would make one naively conclude that such vesicles would become more stable in flow. This observation is not borne by our simulations. Indeed, if one looks at Fig. 5, we instead observe the viscosity ratio $\lambda = 5.0$ vesicle has a lower critical capillary number, i.e., more unstable, than an equiviscous $\lambda = 1$ vesicle. The origin of this counterintuitive observation is likely due to a change in shape. We see in Fig. 6(b) that the shape near shear flow starts developing small off-center cusps resulting in an S-like shape, as is seen for prolate vesicles in shear flow [41]. We emphasize that the vesicle is no longer symmetrical here. The S-like shapes are less prominent in higher viscosity ratio vesicles (Fig. 8), and it appears that when such cusps are absent, the stability trend follows the same trends as $\alpha \geqslant 0.500$ cases.

However, the shape deviation seen in Fig. 6 is a relatively small change, and it does not change drastically even with large differences in viscosity ratio (Fig. 8). To probe the cause for increased vesicle stability for low-α flows, we need to examine the driving force that increases the sinusoidal perturbation by pushing the internal fluid from the smaller to the larger ends. We decided to calculate

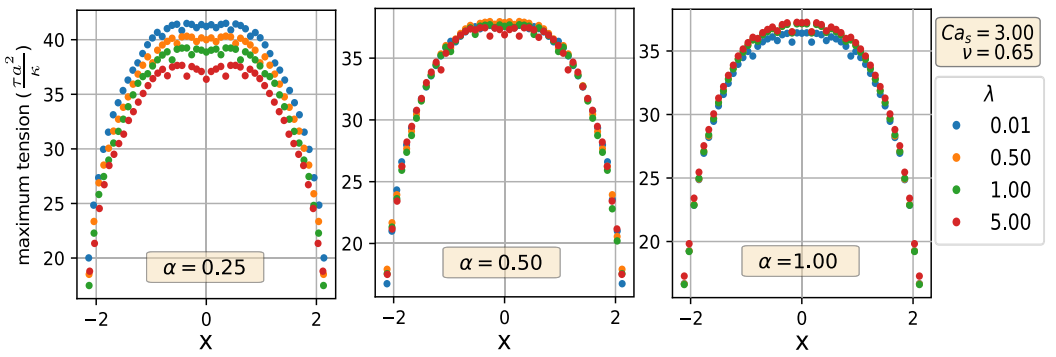

FIG. 7. Maximum tension values along the major axis of the vesicle stationary shape. Note that these are the tensions nondimensionalized by the bending modulus, equivalent to σ Ca. Tension is maximized on the $z = 0$ plane of the vesicle in the planar flow.

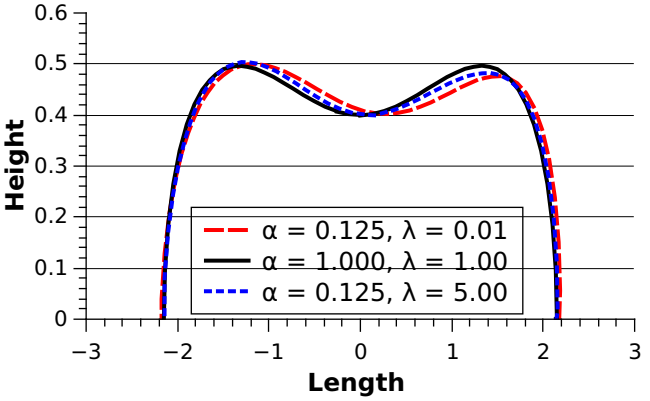

FIG. 8. Upper half of the vesicle stationary shape comparison for $\mathrm{Ca}_s = 2.25$, showing the effect of viscosity ratio. The stationary shape for $\alpha = 0.125$ is shown to deviate from the purely extensional shape (solid line). The increased viscosity ratio vesicle ($\lambda = 5.00$) shows less deviation than the decreased viscosity ratio case ($\lambda = 0.01$).

the pressure profile along the major axis of the vesicle as it is a good indicator of the internal fluid flow. The pressure at a point x_0 inside the vesicle can be calculated using the Green's functions

$$p(\boldsymbol{x}_0) = \frac{-1}{8\pi\lambda}\oint P_i(\boldsymbol{x}_0,\boldsymbol{x})[[f_i]](\boldsymbol{x})dS(\boldsymbol{x}) + \frac{1-\lambda}{8\pi\lambda}\mu_{\text{ext}}\oint u_i(\boldsymbol{x})\Pi_{ij}(\boldsymbol{x}_0,\boldsymbol{x})n_j(\boldsymbol{x})dS(\boldsymbol{x}), \tag{16}$$

$$P_i = \frac{2\hat{x}_i}{r^3}, \quad \Pi_{ij} = 4\left(-\frac{\delta_{ik}}{r^3} + 3\frac{\hat{x}_i\hat{x}_j}{r^5}\right), \tag{17}$$

where $\hat{\boldsymbol{x}} = \boldsymbol{x}_0 - \boldsymbol{x}$. We proceed as in Ref. [17] and decompose the pressure as $p = p_B + p_U$, where p_B is the contribution from bending while p_U is from the external flow. We calculate p_B by solving Eq. (8) with $u^\infty = 0$ and then calculate the resultant pressure profile. This profile will include a nonzero tension that minimizes the area divergence of the bending forces. The pressure p_U is calculated similarly by setting $\boldsymbol{f}_b = 0$ such that $[[\boldsymbol{f}]] = \boldsymbol{f}_s$ and is determined by the external flow only.

We use the pressure profiles to examine vesicles at the same effective extension (14) but for different flow types. We keep the effective extension constant rather than the scaled capillary number (15) because our simulations have shown that vesicles in close to shear flows do not always align with the exit streamline. We simulate at $\alpha = [0.125, 0.500, 1.000]$, $\nu = 0.65$, $\lambda = 1.00$, and an effective capillary number (14) of 3.00. These parameters result in an S-like stationary shape at $\alpha = 0.125$ but a symmetric shape at $\alpha = 0.500$ and 1.000. To determine how a shape perturbation affects the internal pressure profile, we examine the pressure difference between the perturbed and stationary configurations. The perturbed pressure profile is measured at times $\sim 0.1/\dot{\epsilon}$ after perturbation to allow transient effects to dissipate and allow the profile to approximate that of the most unstable mode. For an unstable parameter set, we expect the total pressure ($p = p_B + p_U$) difference profile to give an internal flow that increases the perturbation, in other words, to be positive on the left half of the vesicle and negative on the right for the schematic in Fig. 9. We observe for all simulations that the bending contributions p_B are stabilizing while the flow contributions p_U are destabilizing, which is as expected.

Our calculations show that the pressure difference profiles for $\alpha = 0.5$ and $\alpha = 1.0$ vesicles are very similar, which is further confirmation that flow types not close to shear can be explained by the previously proposed scaling. For the close to shear flow case ($\alpha = 0.125$) however, the total pressure profile shows a stable configuration, suggesting an increased stability at the same effective capillary number. The increased external flow vorticity here results in a decreased destabilizing

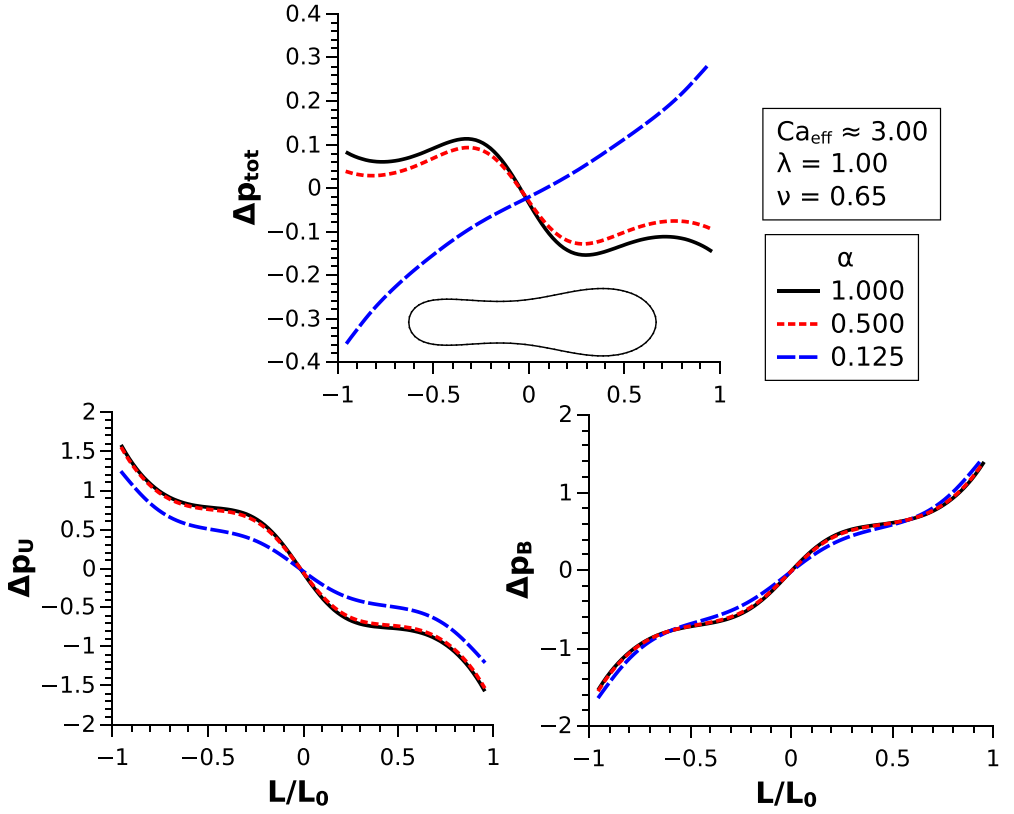

FIG. 9. Difference in pressure profiles between the stationary and perturbed configurations along the major axis of the vesicle. The Ca_{eff} is defined in Eq. (14); Ca_{eff} is approximately 3.00 because the orientation angle of the vesicles is not known *a priori*. The exact Ca_{eff} for the $\alpha = [0.125, 0.500, 1.00]$ are [2.982, 3.006, 3.000], respectively. Note that $Ca_{eff} \approx Ca_s$ for the $\alpha = 0.500$ and 1.000 simulations. The inset shows the exaggerated perturbed shape for reference.

external flow contribution and a slightly altered bending contribution. One can see from Fig. 10 that the tension profile for $\alpha = 0.125$ shows lower values, suggesting that the altered external flow contribution originates from this decreased tension since $\Delta p_U \sim \sigma \Delta H$ [18]. It is interesting that the stabilizing effect from the cusps or their interaction with the sinusoidal perturbation is due to changes in flow forces rather than bending forces. This indicates that if such cusped shapes exist for other soft membrane systems like red blood cells, a similar mechanism may occur to describe their stability in flow, even if the membrane mechanics are more closely dominated by shear elasticity than bending. This shape deviation may also be a major factor in why red blood cells and other similar cellular systems have not been observed to break up in shear flows even with large strain rates. It would be interesting to test these conjectures through simulations and experiments.

IV. CONCLUSION

We have used a boundary element method to evaluate the stability of deflated vesicles in general linear flows. Our simulations agree with previous literature results for planar extensional flow. After introducing the rotational flow component, we observed that most of the mixed flow phase space can be explained by a scaled extensional rate, i.e., a scaled capillary number $Ca_s = \sqrt{\alpha}Ca$, where α is the flow parameter defined in Eq. (4) and Ca is a bending capillary number. For $\alpha \geqslant 0.500$,

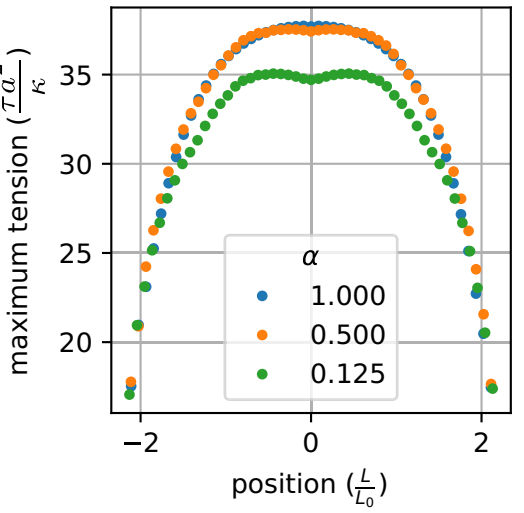

FIG. 10. Stationary shape maximum tension profile for the pressure difference simulations. Note also the nondimensionalization by the bending modulus (see Fig. 7). Here $Ca_{eff} \approx 3.00$, $\lambda = 1.00$, and $\nu = 0.65$.

vesicles at the same scaled capillary number Ca_s have nearly the same shape and tension profile for the simulated viscosity ratios (0.01–5.00) and reduced volumes (0.60–0.70). This is because the vesicles all align very closely with the exiting streamline and the vesicle's internal flows do not stretch the material elements in the membrane appreciably. In this regime, one can accurately quantify the shape and stability of vesicles for a wide range of flow types and viscosity ratios using the results from an equiviscous vesicle under pure extension [18].

For flows close to pure shear flow ($\alpha \leqslant 0.25$), we observed that vesicle stability depends significantly on flow type and viscosity ratio, with the critical capillary number diverging at pure shear flow ($\alpha = 0$). In this flow regime, vesicles develop an S-like shape and exhibit lower tensions at similar effective extension rates. We noted that the presence of such S-like shapes depend on the internal viscosity of the vesicle and only occur if the viscosity ratio is not too large, which explains why this parameter plays a crucial role in this regime. It will be interesting to know if such ideas hold for other soft membrane systems like red blood cells, where the membrane mechanics are more closely dominated by shear contributions rather than bending.

ACKNOWLEDGMENT

The authors would like to thank Dr. Andrew Spann for helpful discussions during preparation of this paper.

[1] M. I. Angelova and D. S. Dimitrov, Liposome electroformation, Faraday Discuss. Chem. Soc. **81**, 303 (1986).

[2] R. Dimova, S. Aranda, N. Bezlyepkina, V. Nikolov, K. A. Riske, and R. Lipowsky, A practical guide to giant vesicles. Probing the membrane nanoregime via optical microscopy, J. Phys.: Condens. Matter **18**, S1151 (2006).

[3] P. M. Vlahovska, T. Podgorski, and C. Misbah, Vesicles and red blood cells in flow: From individual dynamics to rheology, C. R. Phys. **10**, 775 (2009).

[4] B. Kaoui, G. Biros, and C. Misbah, Why Do Red Blood Cells have Asymmetric Shapes Even in a Symmetric Flow? Phys. Rev. Lett. **103**, 188101 (2009).

[5] M. Abkarian and A. Viallat, Vesicles and red blood cells in shear flow, Soft Matter **4**, 653 (2008).
[6] B. Alberts, A. Johnson, J. Lewis, M. Raff, K. Roberts, and P. Walter, *Molecular Biology of the Cell*, 4th ed. (Garland Science, New York, 2002).
[7] C. Settembre, A. Fraldi, D. L. Medina, and A. Ballabio, Signals for the lysosome: A control center for cellular clearance and energy metabolism, Nat. Rev. Mol. Cell Biol. **14**, 283 (2013).
[8] G. Raposo and W. Stoorvogel, Extracellular vesicles: Exosomes, microvesicles, and friends, J. Cell Biol. **200**, 373 (2013).
[9] G. Gregoriadis, Engineering liposomes for drug delivery: Progress and problems, Trends Biotechnol. **13**, 527 (1995).
[10] R. Muzzalupo and L. Tavano, Niosomal drug delivery for transdermal targeting: Recent advances, Res. Rep. Transdermal Drug Deliv. **4**, 23 (2015).
[11] V. Noireaux and A. Libchaber, A vesicle bioreactor as a step toward an artificial cell assembly, Proc. Natl. Acad. Sci. USA **101**, 17669 (2004).
[12] M. Karlsson, M. Davidson, R. Karlsson, A. Karlsson, J. Bergenholtz, Z. Konkoli, A. Jesorka, T. Lobovkina, J. Hurtig, M. Voinova, and O. Orwar, Biomimetic nanoscale reactors and networks, Annu. Rev. Phys. Chem. **55**, 613 (2004).
[13] K. Khairy and J. Howard, Minimum-energy vesicle and cell shapes calculated using spherical harmonics parameterization, Soft Matter **7**, 2138 (2011).
[14] V. Kantsler, E. Segre, and V. Steinberg, Critical Dynamics of Vesicle Stretching Transition in Elongational Flow, Phys. Rev. Lett. **101**, 048101 (2008).
[15] J. Spjut, Trapping, deformation, and dynamics of phospholipid vesicles, Ph.D. thesis, University of California, Berkeley, 2010.
[16] J. B. Dahl, V. Narsimhan, B. Gouveia, S. Kumar, E. S. G. Shaqfeh, and S. J. Muller, Experimental observation of the asymmetric instability of intermediate-reduced-volume vesicles in extensional flow, Soft Matter **12**, 3787 (2016).
[17] H. Zhao and E. S. G. Shaqfeh, The shape stability of a lipid vesicle in a uniaxial extensional flow, J. Fluid Mech. **719**, 345 (2013).
[18] V. Narsimhan, A. Spann, and E. Shaqfeh, The mechanism of shape instability for a vesicle in extensional flow, J. Fluid Mech. **750**, 144 (2014).
[19] V. Narsimhan, A. Spann, and E. Shaqfeh, Pearling, wrinkling, and buckling of vesicles in elongational flows, J. Fluid Mech. **777**, 1 (2015).
[20] A. P. Spann, H. Zhao, and E. S. G. Shaqfeh, Loop subdivision surface boundary integral method simulations of vesicles at low reduced volume ratio in shear and extensional flow, Phys. Fluids **26**, 031902 (2014).
[21] J. Deschamps, V. Kantsler, and V. Steinberg, Phase Diagram of Single Vesicle Dynamical States in Shear Flow, Phys. Rev. Lett. **102**, 118105 (2009).
[22] A. Farutin, T. Biben, and C. Misbah, Analytical progress in the theory of vesicles under linear flow, Phys. Rev. E **81**, 061904 (2010).
[23] D. Barthès-Biesel and A. Acrivos, Deformation and burst of a liquid droplet freely suspended in a linear shear field, J. Fluid Mech. **61**, 1 (1973).
[24] B. J. Bentley and L. G. Leal, An experimental investigation of drop deformation and breakup in steady, two-dimensional linear flows, J. Fluid Mech. **167**, 241 (1986).
[25] W. Rawicz, K. Olbrich, T. McIntosh, D. Needham, and E. Evans, Effect of chain length and unsaturation on elasticity of lipid bilayers, Biophys. J. **79**, 328 (2000).
[26] J. Henriksen and J. Ipsen, Measurement of membrane elasticity by micro-pipette aspiration, Eur. Phys. J. E **14**, 149 (2004).
[27] W. Helfrich, Elastic properties of lipid bilayers: Theory and possible experiments, Z. Naturforsch. C **28**, 693 (1973).
[28] H. Zhao and E. S. G. Shaqfeh, The dynamics of a vesicle in simple shear flow, J. Fluid Mech. **674**, 578 (2011).
[29] G. Boedec, M. Leonetti, and M. Jaeger, 3D vesicle dynamics simulations with a linearly triangulated surface, J. Comput. Phys. **230**, 1020 (2011).

[30] H.-G. Dobereiner, O. Selchow, and R. Lipowsky, Spontaneous curvature of fluid vesicles induced by trans-bilayer sugar asymmetry, Eur. Biophys. J. **28**, 174 (1999).
[31] H. Deuling and W. Helfrich, The curvature elasticity of fluid membranes: A catalog of vesicle shapes, J. Phys. (Paris) **37**, 1335 (1976).
[32] L. Bagatolli and P. B. Sunil Kumar, Phase behavior of multicomponent membranes: Experimental and computational techniques, Soft Matter **5**, 3234 (2009).
[33] U. Seifert, Configurations of fluid membranes and vesicles, Adv. Phys. **46**, 13 (1997).
[34] H. Noguchi and G. Gompper, Dynamics of fluid vesicles in shear flow: Effect of membrane viscosity and thermal fluctuations, Phys. Rev. E **72**, 011901 (2005).
[35] H. Zhao and E. S. Shaqfeh, The dynamics of a non-dilute vesicle suspension in a simple shear flow, J. Fluid Mech. **725**, 709 (2013).
[36] M. Loewenberg and E. J. Hinch, Numerical simulation of a concentrated emulsion in shear flow, J. Fluid Mech. **321**, 395 (1996).
[37] A. J. C. Moreira and Y. M. Santos, Concave hull: A k-nearest neighbors approach for the computation of the region occupied by a set of points, in *Proceedings of the Second International Conference on Computer Graphics Theory and Applications- Volume 2: GRAPP* (SciTePress, 2007), pp. 61–68.
[38] H. Karam and J. Bellinger, Deformation and breakup of liquid droplets in a simple shear field, Ind. Eng. Chem. Fund. **7**, 576 (1968).
[39] H. A. Stone, Dynamics of drop deformation and breakup in viscous fluids, Annu. Rev. Fluid Mech. **26**, 65 (1994).
[40] C. Misbah, Vacillating Breathing and Tumbling of Vesicles Under Shear Flow, Phys. Rev. Lett. **96**, 028104 (2006).
[41] H. Zhao, A. P. Spann, and E. S. G. Shaqfeh, The dynamics of a vesicle in a wall-bound shear flow, Phys. Fluids **23**, 121901 (2011).
[42] P. M. Vlahovska and R. S. Gracia, Dynamics of a viscous vesicle in linear flows, Phys. Rev. E **75**, 016313 (2007).
[43] S. R. Keller and R. Skalak, Motion of a tank-treading ellipsoidal particle in a shear flow, J. Fluid Mech. **120**, 27 (1982).